Directional tunnelling spectroscopy of a normal metal–s + g-wave superconductor junction

2003 J. Phys.: Condens. Matter 15 4457

(http://iopscience.iop.org/0953-8984/15/25/313)

INSTITUTE OF PHYSICS PUBLISHING JOURNAL OF PHYSICS: CONDENSED MATTER

J. Phys.: Condens. Matter **15** (2003) 4457–4468 PII: S0953-8984(03)60557-6

Directional tunnelling spectroscopy of a normal metal–s + g-wave superconductor junction

P Pairor[1] **and M F Smith**[2]

[1] School of Physics, Institute of Science, Suranaree University of Technology, 111 University Avenue, Nakhon Ratchasima, 30000, Thailand
[2] Department of Physics, University of Toronto, 60 St George Street, Toronto, ON, M5S 1A7, Canada

E-mail: pairor@ccs.sut.ac.th

Received 6 March 2003
Published 13 June 2003
Online at stacks.iop.org/JPhysCM/15/4457

Abstract

We calculate the normal metal–s + g-wave superconductor tunnelling spectrum for various junction orientations and for two forms of the superconducting gap, one which allows for point nodes and the other which allows for line nodes. For a junction oriented with its normal parallel to the *ab* plane of the tetragonal superconductor, we find that the tunnelling spectrum is strongly dependent on orientation in the plane. The spectrum contains two peaks at energies equivalent to the magnitudes of the gap function in the direction parallel to the interface normal and in the direction making a $\pi/4$ angle with the normal. These two peaks appear in both superconductors with point nodes and line nodes, but are more prominent in the latter. For the tunnelling along the *c* axis, we find a sharp peak at the gap maximum in the conductance spectrum of the superconductor with line nodes, whereas with point nodes we find a peak occurring at the value of the gap function along the *c* axis. We discuss the relevance of our result to borocarbide systems.

(Some figures in this article are in colour only in the electronic version)

1. Introduction

Nonmagnetic rare-earth borocarbides, such as YNi_2B_2C and $LuNi_2B_2C$, are among the materials which exhibit unconventional superconductivity. There is strong evidence in these materials indicating that their superconducting gap function is highly anisotropic [1, 2] and that there exist low-lying excitations in the superconducting state [3–8]. The presence of these low-energy excitations implies that the gap function has nodes (or deep minima) on the Fermi surface. The location of these nodes and their nature, i.e., whether they are point nodes or line nodes, is still unclear. The thermal conductivity in a magnetic field at low temperatures [1] and the dependence of the specific heat on the magnetic field [3, 6] suggest the existence of line nodes like those in the cuprates and UPt_3. However, the recent measurements of the

c-axis thermal conductivity in a rotational magnetic field along the ab plane were interpreted as evidence for a gap function with point nodes along [100] and [010] directions [2]. Further studies which employ different experimental techniques may be necessary to determine the detailed structure of the superconducting gap function in momentum space. Here we suggest that directional tunnelling spectroscopy may be useful for this purpose.

In general, the tunnelling conductance spectrum of an anisotropic superconductor is strongly dependent on the crystal orientation with respect to the interface plane. In the case of a d-wave superconductor with vertical line nodes, it has been shown that features in the conductance spectrum occur at voltages which depend strongly on crystal orientation. These voltages correspond to values of the gap function at particular points on the Fermi surface [9]. For instance, in the case of an ab-plane tunnelling junction, if the surface orientation of the superconductor is not [100] or [010], the conductance spectrum contains a peak at the voltage corresponding to the value of the gap function in the direction parallel to the surface normal. The observation of this feature would, in principle, allow the directional normal metal–superconductor (NS) tunnelling spectroscopy to map out the magnitude of the superconducting gap function.

In this paper, we calculate the NS tunnelling spectra of anisotropic s-wave superconductors with two forms of gap functions, which have been suggested as possible candidates for the gap in borocarbides [10, 11]. The candidates are allowed by the symmetry of the borocarbide crystal structure and consistent with experimental results. It is apparent that the gap function has fourfold symmetry and does not change sign, but there is evidence for deep minima along [100] and [010] directions [1–8]. The simplest suitable candidates are of the s + g-wave form. In our calculation, we find, similar to a d-wave case, that features appear in the spectra at voltages corresponding to values of the gap at particular points on the Fermi surface depending on surface orientation. Some of these features are characteristic of the general s + g-wave gap function and are thus common to the two candidates, while one particular feature occurs only for the candidate with point nodes. Thus, if these features can be observed experimentally, it may be possible to determine which form of the gap, if either, correctly describes that of the borocarbides.

The two candidate gap functions are both s + g-wave and are given by equations (1a) and (1b) respectively:

$$\Delta_{k,1} = \Delta_s - \Delta_g \cos 4\phi \tag{1a}$$

$$\Delta_{k,2} = \Delta_s - \Delta_g \sin^2\theta \cos 4\phi \tag{1b}$$

where θ and ϕ are the polar angles in spherical coordinates, and Δ_s and Δ_g are the s and g components of the gap function respectively. For an elliptical Fermi surface, the case of line (point) nodes occurs when $\Delta_s = \Delta_g$ in equations (1a), (1b). We study both ab-plane and c-axis tunnelling spectra for both forms of the gap function by using the so-called Blonder–Tinkham–Klapwijk (BTK) scattering formalism [12] and a continuous model to describe the electronic structure of the normal metal and superconductor. Although detailed features of the conductance depend on the shape of the Fermi surface, it is sufficient to use the continuous model which gives an elliptical Fermi surface to study the positions of the main features in the conductance spectra [9].

In the case of tunnelling into the ab plane of a s + g-wave superconductor, we show in this paper that there are three main features occurring at voltages associated with the difference of the s and g components of the gap function and the values of the gap function in two particular directions with respect to the interface normal, one in the direction parallel to the surface normal and the other in the direction making a $\pi/4$ angle with the surface normal. These two features are more prominent for the s + g-wave superconductor with line nodes than for

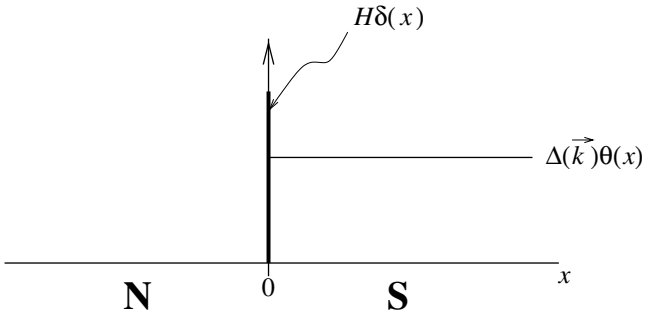

Figure 1. The NS junction is represented by an infinite system as shown in this picture. The normal metal fills the $x < 0$ region and the superconductor fills the $x > 0$ region. The insulator layer is represented by a delta function of height H in units of energy per length. The gap function is taken to be zero in the normal metal and to be nonzero and independent of x in the superconductor.

the superconductor with point nodes. In the case of c-axis tunnelling junctions, there is one prominent feature at the maximum gap in the conductance spectrum of the superconductor with line nodes, whereas for the superconductor with point nodes the conductance spectrum contains two features, one at the maximum gap and the other at the value of the gap function along the c axis.

In section 2, we describe the calculation method and the assumptions used throughout this paper. Then, we provide the detailed results and discussion of all the cases of interest at zero temperature in section 3. In addition to the cases in which the nodes exist, we also consider cases in which the superconducting gap has small but nonzero gap minima. We show all the results in both the Andreev limit (low barrier) and the tunnelling limit (high barrier).

2. Assumptions and method of calculation

As in [12], we represent the NS junction with an infinite system, the left half of which is a normal metal and the right half of which is a superconductor (see figure 1). The insulating barrier is represented by a delta function potential with strength H. For the ab-plane tunnelling junctions, the interface normal vector lies somewhere in the ab plane, and for the c-axis tunnelling junction the interface normal is parallel to the c axis.

We take the normal metal to be cubic, and take the superconductor to be tetragonal to describe the crystal structure of the borocarbides. In our calculation, we ignore both the suppression of the gap function near the NS interface and the proximity effect for simplicity. The gap function Δ_k is taken to be as in either equations (1a) or (1b).

The Bogoliubov–de Gennes equations that describe the excitations of the system are

$$\begin{bmatrix} \hat{O}_p + H\delta(x) - \mu & \Delta_k\Theta(x) \\ \Delta_k\Theta(x) & -\hat{O}_p - H\delta(x) + \mu \end{bmatrix} U(\vec{r}) = EU(\vec{r}) \tag{2}$$

where μ is the chemical potential, $\Theta(x)$ is the Heaviside step function,

$$\hat{O}_p = -\frac{\hbar^2}{2}\left(\frac{1}{m_{xy}}\left(\frac{\partial^2}{\partial x^2} + \frac{\partial^2}{\partial y^2}\right) + \frac{1}{m_z}\frac{\partial^2}{\partial z^2}\right),$$

$$m_{xy} = \begin{cases} m \text{ (effective mass in the normal metal)}, & x < 0, \\ m_{ab} \ (ab\text{-plane effective mass in the superconductor)}, & x > 0, \end{cases}$$

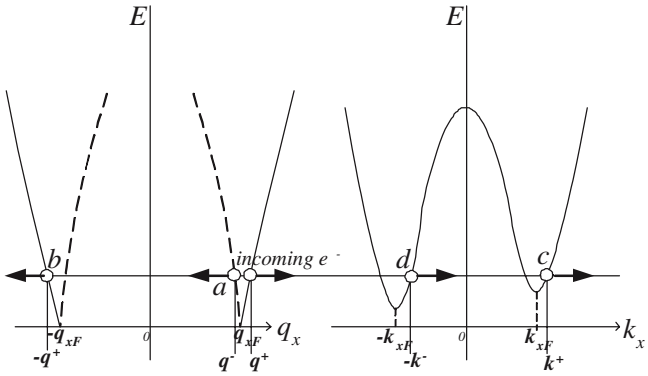

Figure 2. The plots of two excitation energies as a function of q_x or k_x, the component parallel to the interface normal, at a particular value of $\vec{k}_\parallel$, which is (k_y, k_z). The plot on the left is for the excitation energy of the normal metal and the plot on the right is for the excitation energy of the superconductor. At the same energy, there can be four propagating excitations for each side. However, for an electron incoming from the normal side, the wavefunction of the normal metal is a linear combination of only three excitations represented by the open circles, and the wavefunction of the superconductor is the sum of two outgoing excitations also represented by the open circles.

$$m_z = \begin{cases} m, & x < 0, \\ m_c \ (c\text{-axis effective mass in the superconductor}), & x > 0, \end{cases}$$

and $U(\vec{r})$ is a two-component function:

$$U(\vec{r}) = \begin{bmatrix} u(\vec{r}) \\ v(\vec{r}) \end{bmatrix} = \begin{bmatrix} u_k \\ v_k \end{bmatrix} \mathrm{e}^{\mathrm{i}\vec{k}\cdot\vec{r}}. \tag{3}$$

After substituting $U(\vec{r})$ from equation (3) into (2), we obtain the bulk excitation energies for the normal metal and superconductor respectively as

$$E(\vec{q}) = \pm\xi_q = \pm\left(\frac{\hbar^2}{2m}(q_x^2 + q_y^2 + q_z^2) - \mu\right) \tag{4a}$$

$$E(\vec{k}) = \sqrt{\xi_k^2 + \Delta_k^2} \tag{4b}$$

where for the normal metal (equation (4*a*)) the plus and minus signs are for electron and hole excitations respectively, and for the superconductor (equation (4*b*))

$$\xi_k = \frac{\hbar^2}{2}\left(\frac{k_x^2 + k_y^2}{m_{ab}} + \frac{k_z^2}{m_c}\right) - \mu. \tag{5}$$

Figure 2 shows a plot of the excitation energy of the normal metal (superconductor) as a function of q_x (k_x), the component along the interface normal, at a particular $\vec{q}_\parallel = \vec{k}_\parallel = (k_y, k_z)$, the component perpendicular to the interface normal.

The amplitudes of the excitations, u_k and v_k, of the normal metal are

$$\begin{bmatrix} u_k \\ v_k \end{bmatrix} = \begin{cases} \begin{bmatrix} 1 \\ 0 \end{bmatrix} & \text{for electrons,} \\ \begin{bmatrix} 0 \\ 1 \end{bmatrix} & \text{for holes,} \end{cases} \tag{6}$$

whereas those of the superconductor are

$$\begin{bmatrix} u_k \\ v_k \end{bmatrix} = \frac{1}{\sqrt{|E + \xi_k|^2 + \Delta_k^2}} \begin{bmatrix} \Delta_k \\ E + \xi_k \end{bmatrix}. \tag{7}$$

The wavefunction of each side is a linear combination of all the appropriate excitations of the same energy and the momentum that has the same component perpendicular to the interface normal. For ab-plane tunnelling, the wavefunctions of both sides are therefore

$$U_N(\vec{r}) = \left(\begin{bmatrix} 1 \\ 0 \end{bmatrix} e^{iq^+x} + a \begin{bmatrix} 0 \\ 1 \end{bmatrix} e^{iq^-x} + b \begin{bmatrix} 1 \\ 0 \end{bmatrix} e^{-iq^+x} \right) e^{ik_y y + ik_z z} \tag{8a}$$

$$U_S(\vec{r}) = \left(c \begin{bmatrix} u_{k^+} \\ v_{k^+} \end{bmatrix} e^{ik^+x} + d \begin{bmatrix} u_{-k^-} \\ v_{-k^-} \end{bmatrix} e^{-ik^-x} \right) e^{ik_y y + ik_z z} \tag{8b}$$

where $q^\pm$ and $k^\pm$ (see figure 2) satisfy

$$\hbar q^\pm = \sqrt{2m(\mu \pm E) - \hbar^2 k_y^2 - \hbar^2 k_z^2} \tag{9a}$$

$$\frac{\hbar k^\pm}{\sqrt{m_{ab}}} = \sqrt{2\left(\mu \pm \sqrt{E^2 - \Delta_k^2}\right) - \frac{\hbar^2 k_y^2}{m_{ab}} - \frac{\hbar^2 k_z^2}{m_c}} \tag{9b}$$

and a, b, c, and d are the Andreev reflection, the normal reflection, the same-branched transmission, and the cross-branched transmission amplitudes respectively. For the c-axis tunnelling, we can obtain the wavefunction of each side in a similar way.

Normally, the range of the energy E relevant to the NS tunnelling experiments is of meV order whereas the Fermi energy is of eV order. Therefore, we use the following approximation for $q^\pm$ and $k^\pm$:

$$q^+ = q^- = \sqrt{\frac{2m\mu}{\hbar^2} - k_y^2 - k_z^2} = q_F \sin\theta_N \cos\phi_N \tag{10a}$$

$$k^+ = k^- = k_F \sqrt{\frac{m_{ab}}{m^*}} \sin\theta_S \cos\phi_S \tag{10b}$$

where q_F is the magnitude of the Fermi wavevector of the normal metal, and k_F, m^* are the parameters that satisfy $\hbar^2 k_F^2/(2m^*) = E_{F,S}$, the Fermi energy of the superconductor. Using the conservation of the momentum parallel to the surface, we have the following relationship between the polar angles in spherical coordinates:

$$q_F \sin\theta_N \sin\phi_N = k_F \sqrt{\frac{m_{ab}}{m^*}} \sin\theta_S \sin\phi_S \tag{11a}$$

$$q_F \cos\theta_N = k_F \sqrt{\frac{m_c}{m^*}} \cos\theta_S. \tag{11b}$$

We obtain all the amplitudes a, b, c, and d by applying the following matching conditions at the interface:

$$U_N(x=0) = U_S(x=0) \equiv U_0 \tag{12a}$$

$$ZU_0 = \frac{1 + m/m_{ab}}{4k_F} \left(\left.\frac{\partial U_S}{\partial x}\right|_{x=0^+} - \left.\frac{\partial U_N}{\partial x}\right|_{x=0^-} \right) \tag{12b}$$

where $Z = mH/(\hbar^2 k_F)$. Note that both matching conditions are for the ab-plane tunnelling junction. For the c-axis tunnelling junction, the first condition remains the same, but we have to replace m_{ab} with m_c in the second condition.

In the BTK formalism, the Andreev reflection, the normal reflection, and the two transmission probabilities are used to obtain the current across the junction. All the reflection and transmission probabilities are obtained from

$$A = |a|^2 \left(\frac{q^-}{q^+} \right) \tag{13a}$$

$$B = |b|^2 \tag{13b}$$

$$C = |c|^2(|u_{k^+}|^2 - |v_{k^+}|^2)\left(\frac{k^+}{q^+}\right) \tag{13c}$$

$$D = |d|^2(|u_{-k^-}|^2 - |v_{-k^-}|^2)\left(\frac{k^-}{q^+}\right) \tag{13d}$$

and satisfy $A + B + C + D = 1$, i.e., the number of particles is conserved.

On the normal metal side, we find that the current across the junction as a function of an applied voltage is

$$I_{NS}(V) = \frac{e\Omega}{(2\pi)^3}\int \mathrm{d}\vec{q}\, v_{q_x}[1 + A(\vec{q}) - B(\vec{q})][f(E_q - eV) - f(E_q)] \tag{14}$$

where Ω is volume, v_{q_x} is the x component of the group velocity of the incoming electron, and $f(E)$ is the Fermi–Dirac distribution function. The conductance of the ab-plane junction at zero temperature is

$$G_{NS}^{ab}(V) = \frac{\mathrm{d}I_{NS}^{ab}}{\mathrm{d}V} = \frac{me^3\Omega V}{4\pi^2\hbar^2}\int \mathrm{d}\phi_N \int \mathrm{d}\theta_N \sin^2\theta_N \cos\phi_N \times [1 + A(V, \phi_N, \theta_N) - B(V, \phi_N, \theta_N)]. \tag{15}$$

Similarly, the conductance of the c-axis tunnelling junction is

$$G_{NS}^{c}(V) = \frac{me^3\Omega V}{4\pi^2\hbar^2}\int \mathrm{d}\phi_N \int \mathrm{d}\theta_N \sin\theta_N \cos\theta_N[1 + A(V, \phi_N, \theta_N) - B(V, \phi_N, \theta_N)]. \tag{16}$$

The limits of both integrals can be found by considering equations (11a) and (11b).

3. Results and discussion

We plot the normalized conductance as a function of applied voltage for both ab-plane and c-axis tunnelling. We define the normalized conductance as the conductance of the junction normalized by its value at a high voltage, i.e., $eV \gg \Delta_{max}$, the maximum magnitude of the gap function. Using both forms of the gap function in equations (1a) and (1b), we consider three cases: (1) $\Delta_s = \Delta_g$, (2) $\Delta_s = 0.9\Delta_g$, and (3) $\Delta_s = 1.1\Delta_g$. These choices of the parameter Δ_s/Δ_g span the range allowed by the results of thermal conductivity measurements in borocarbides which indicate that the ratio of the gap maximum to the gap minimum is at least 10 [1]. All the results are obtained for zero temperature.

3.1. ab-plane tunnelling

Figure 3 shows the diagram of the junction that has the interface normal on the ab plane of the superconductor. We specify the orientation in the ab plane with α, the angle between the interface normal and the a axis of the superconductor. The gap function is a function of α:

$$\Delta_{k^\pm,1} = \Delta_s - \Delta_g \cos 4(\phi_S \mp \alpha) \tag{17a}$$

$$\Delta_{k^\pm,2} = \Delta_s - \Delta_g \sin^2\theta_S \cos 4(\phi_S \mp \alpha). \tag{17b}$$

In the Andreev limit (small Z), the conductance spectrum depends very little on the junction orientation. As shown in figure 4 for $\Delta_{k,1}$ and in figure 5 for $\Delta_{k,2}$, the conductance spectra in all cases have the inverted gap structure. Note that in the case of $\Delta_{k,2}$ in figure 5, there is a slight kink at the voltage associated with the value of the gap function along the c axis ($eV = \Delta_s$). Also note that when $\Delta_s \neq \Delta_g$, there is a feature occurring at $eV = |\Delta_s - \Delta_g|$ as marked by the arrows in figures 4(b), (c) and 5(b), (c).

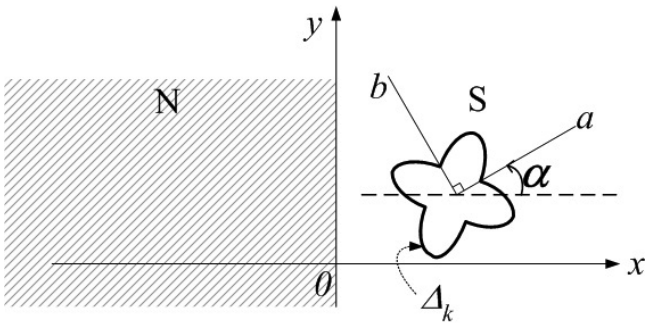

Figure 3. The geometry of the *ab*-plane tunnelling NS junction. The angle between the x axis and the a axis, α, defines the orientation of the junction.

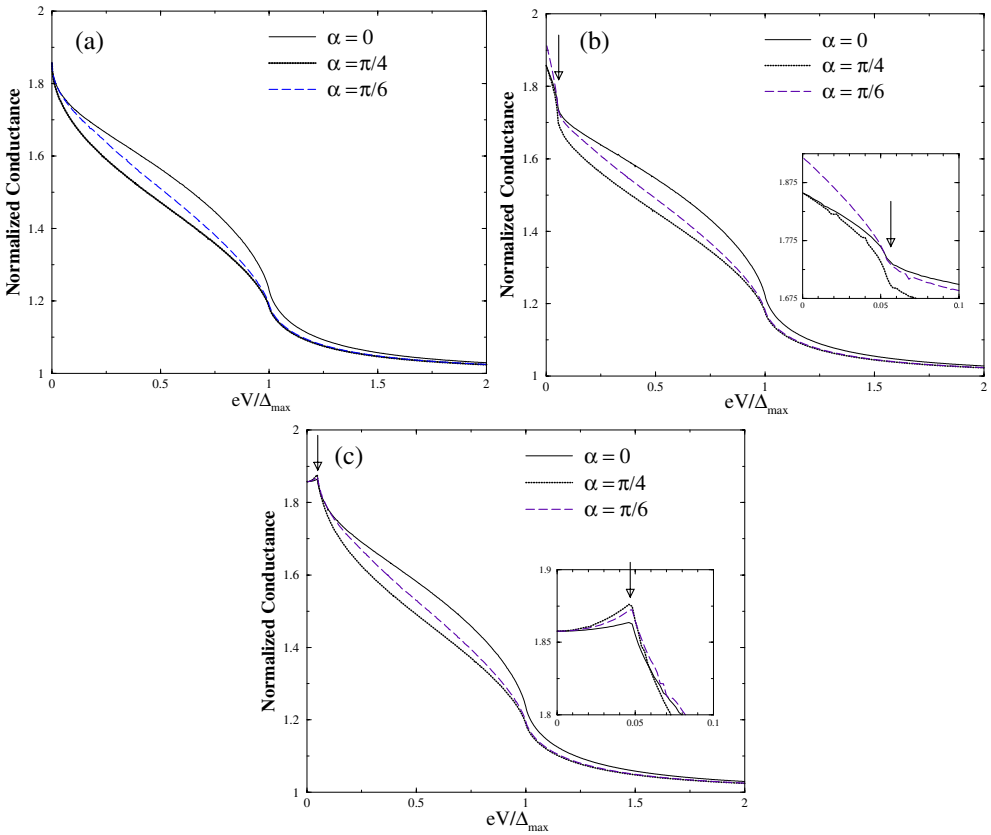

Figure 4. *ab-plane tunnelling junctions.* The plots of the normalized conductance spectra when $Z = 0$ for three surface orientations for three cases of the gap function $\Delta_{k^{\pm},1} = \Delta_s - \Delta_g \cos 4(\phi_S \mp \alpha)$: (a) $\Delta_s = \Delta_g$, (b) $\Delta_s = 0.9\Delta_g$, and (c) $\Delta_s = 1.1\Delta_g$. The arrows in (b) and (c) indicate the feature occurring at the voltage corresponding to $|\Delta_s - \Delta_g|$. The insets in (b) and (c) are enlargements of the conductance plots near zero voltage.

In the tunnelling limit (large Z), the shape of the conductance spectrum changes with the interface orientation. First, consider the case where $\Delta_s = \Delta_g$; there are two distinct peaks which are more pronounced for the superconductor with the gap function $\Delta_{k,1}$ than

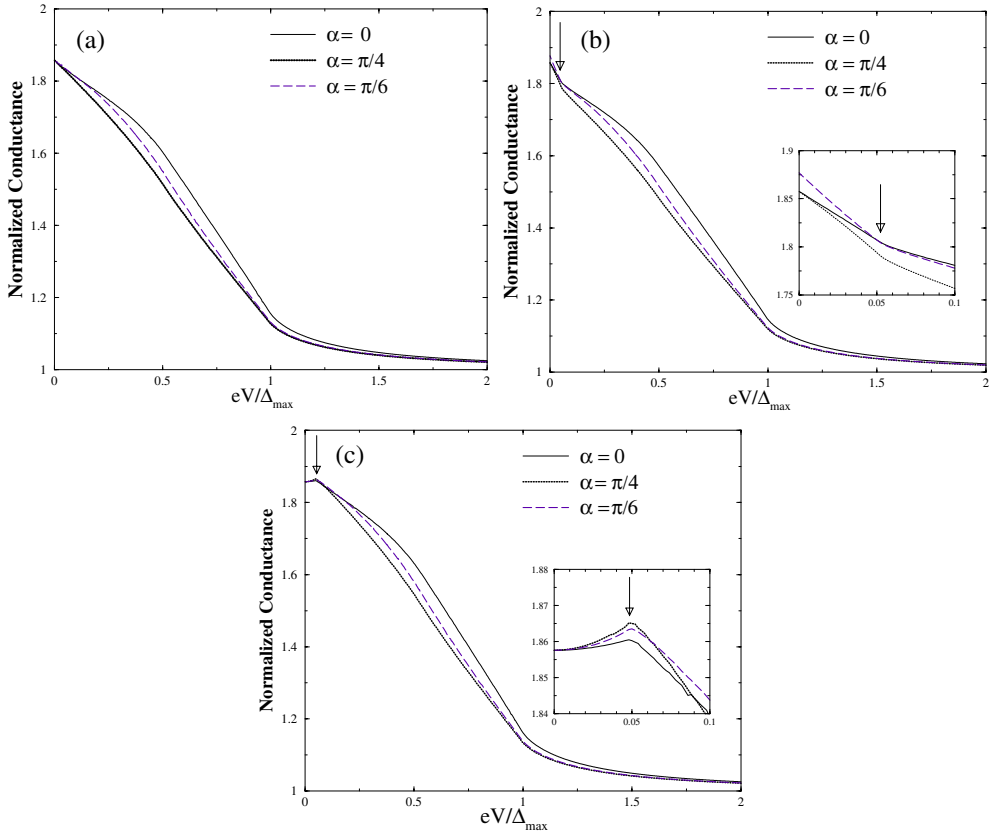

Figure 5. *ab-plane tunnelling junctions.* The plots of the normalized conductance spectra when $Z = 0$ for three surface orientations for three cases of the gap function $\Delta_{k^{\pm},2} = \Delta_s - \Delta_g \sin^2\theta_S \cos 4(\phi_S \mp \alpha)$: (a) $\Delta_s = \Delta_g$, (b) $\Delta_s = 0.9\Delta_g$, and (c) $\Delta_s = 1.1\Delta_g$. The arrows in (b) and (c) indicate the feature occurring at the voltage corresponding to $|\Delta_s - \Delta_g|$. The insets in (b) and (c) are enlargements of the conductance plots near zero voltage.

for the superconductor with the gap function $\Delta_{k,2}$ (compare figures 6(a) and 7(a)). The two peaks occur at voltages corresponding to $\Delta_{k,i}(\theta_S = \pi/2, \phi_S = 0, \alpha)$ (marked by the filled arrows) and $\Delta_{k,i}(\theta_S = \pi/2, \phi_S = \pi/4, \alpha)$ (marked by the hollowed arrows), where i is either 1 or 2. Notice that when $\alpha = \pi/8$, there is only one peak due to the fact that $\Delta_{k,i}(\theta_S = \pi/2, \phi_S = 0, \alpha = \pi/8) = \Delta_{k,i}(\theta_S = \pi/2, \phi_S = \pi/4, \alpha = \pi/8)$.

In the case of $\Delta_s = 0.9\Delta_g$, $\Delta_{k,i}$ can be both positive and negative. Consequently, for the orientations with $\alpha \neq 0, \pi/4$, in addition to the two peaks at the positions like those in the case of $\Delta_s = \Delta_g$, there exists a peak at zero voltage (see figures 6(b) and 7 (b)). The existence of this zero-bias conductance peak, which also occurs in the d-wave case, is a signature of the presence of a sign change of the gap function [13, 14].

When $\Delta_s = 1.1\Delta_g$, there is a finite gap minimum. The conductance is very small for voltages less than the gap minimum, and the two peaks at $\Delta_{k,i}(\theta_S = \pi/2, \phi_S = 0, \alpha)$ and $\Delta_{k,i}(\theta_S = \pi/2, \phi_S = \pi/4, \alpha)$ are still present.

In summary, the conductance spectrum in every case where $\alpha \neq 0, \pi/4$ contains two peaks at $\Delta_{k,i}(\theta_S = \pi/2, \phi_S = 0, \alpha)$ and $\Delta_{k,i}(\theta_S = \pi/2, \phi_S = \pi/4, \alpha)$. These two angles, $\phi_S = 0, \pi/4$, are special because the magnitudes of the gap function of the two transmitted superconducting excitations with the k_y corresponding to these angles are the same, i.e.,

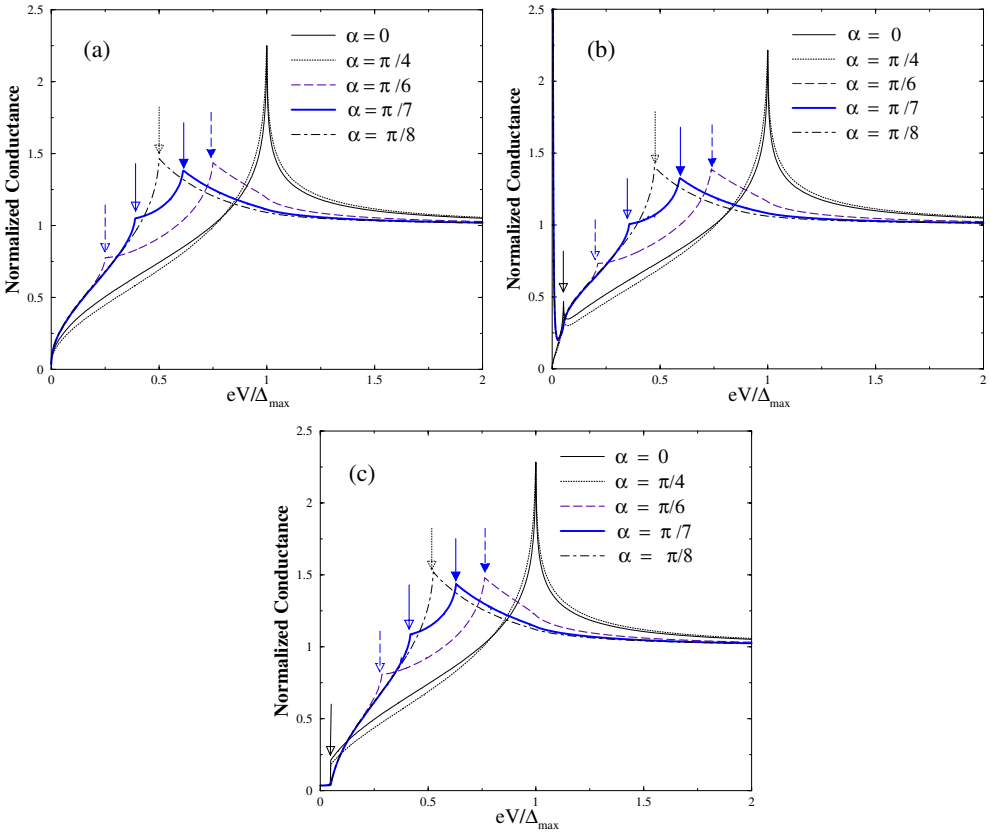

Figure 6. *ab-plane tunnelling junctions.* The plots of the normalized conductance spectra when $Z = 3$ for three interface orientations for three cases of the gap function $\Delta_{k^{\pm},1} = \Delta_s - \Delta_g \cos 4(\phi_S \mp \alpha)$: (a) $\Delta_s = \Delta_g$, (b) $\Delta_s = 0.9\Delta_g$, and (c) $\Delta_s = 1.1\Delta_g$. The hollowed arrows indicate the features occurring at the voltage corresponding to $\Delta_{k,1}(\theta_S = \pi/2, \phi_S = \pi/4, \alpha)$ and the filled arrows mark the features at the voltage corresponding to $\Delta_{k,1}(\theta_S = \pi/2, \phi_S = 0, \alpha)$.

$\Delta_{k^+} = \Delta_{-k^-}$, as shown pictorially in figure 8. The feature at $\Delta_{k,i}(\theta_S = \pi/2, \phi_S = 0, \alpha)$ has also been shown to occur in a d-wave superconductor in a continuous model [9]. However, the feature at $\Delta_{k,i}(\theta_S = \pi/2, \phi_S = \pi/4, \alpha)$ is unique to an anisotropic s-wave superconductor in this model. In a d-wave superconductor the values of $\Delta_{k^+}(\theta_S = \pi/2, \phi_S = \pi/4, \alpha)$ and $\Delta_{-k^-}(\theta_S = \pi/2, \phi_S = \pi/4, \alpha)$ always have opposite signs and thus excitations having these momenta contribute to the zero-energy surface bound state [13] instead of giving rise to such a feature. We note that the two peaks at $\Delta_{k,i}(\theta_S = \pi/2, \phi_S = 0, \alpha)$ and $\Delta_{k,i}(\theta_S = \pi/2, \phi_S = \pi/4, \alpha)$ are more prominent for the superconductor with the gap function $\Delta_{k,1}$ than for the superconductor with the gap function $\Delta_{k,2}$. Given only this quantitative distinction between the *ab*-plane tunnelling results for the two forms of the gap considered, it would probably be difficult to determine from real tunnelling data which form is present. The *ab*-plane tunnelling spectrum would enable a determination of the magnitude of the gap function in an arbitrary direction in the plane for either of the two forms of the gap.

3.2. c-axis tunnelling

Because in the continuous model the Fermi surface of a tetragonal crystal is invariant under rotation around the *c* axis of the crystal, the *c*-axis tunnelling spectroscopy is independent of

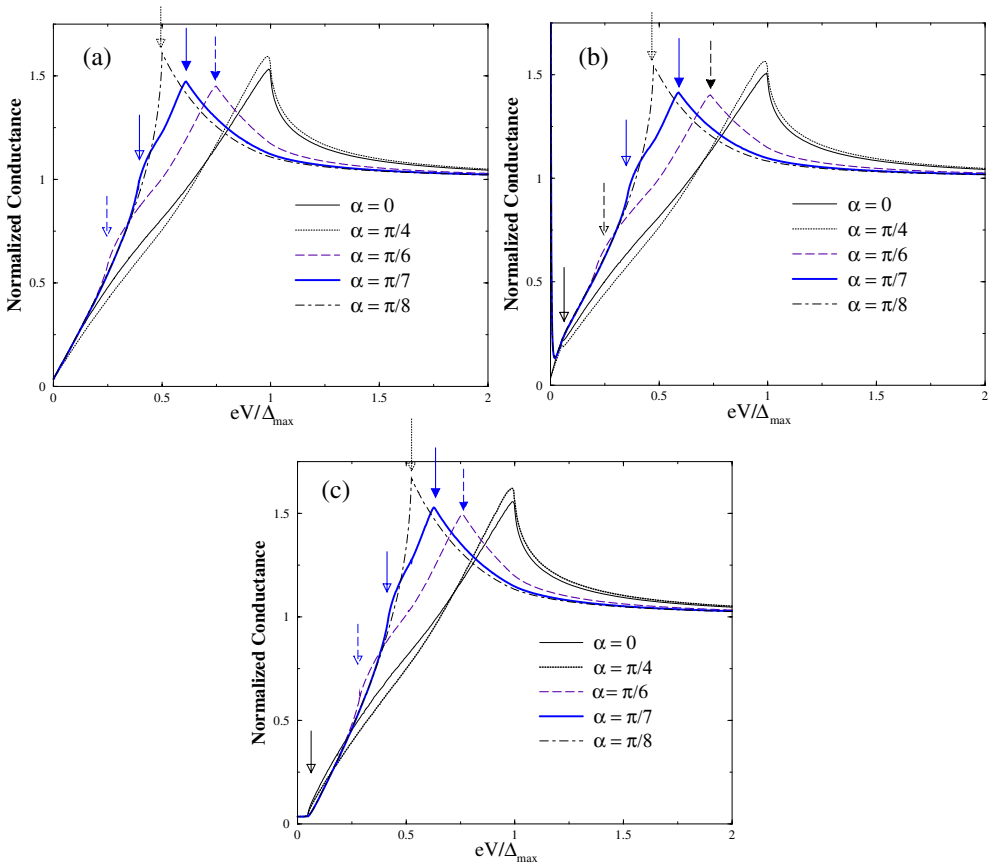

Figure 7. *ab-plane tunnelling junctions.* The plots of the normalized conductance spectra when $Z = 3$ for three interface orientations for three cases of the gap function $\Delta_{k^{\pm},2} = \Delta_s - \Delta_g \sin^2\theta_S \cos 4(\phi_S \mp \alpha)$: (a) $\Delta_s = \Delta_g$, (b) $\Delta_s = 0.9\Delta_g$, and (c) $\Delta_s = 1.1\Delta_g$. The hollowed arrows indicate the features at the voltage corresponding to $\Delta_{k,2}(\theta_S = \pi/2, \phi_S = \pi/4, \alpha)$ and the filled arrows mark the features at the voltage corresponding to $\Delta_{k,2}(\theta_S = \pi/2, \phi_S = 0, \alpha)$.

the rotation around the c axis. In the Andreev limit, when $|\Delta_s - \Delta_g| < eV < \Delta_{max}$, the conductance curve of the superconductor with the gap function $\Delta_{k,1}$ is upward and decreasing smoothly (see figure 9(a)). In contrast, the conductance curve of the superconductor with the gap function $\Delta_{k,2}$ is downward when $|\Delta_s - \Delta_g| < eV < \Delta_{k,2}(\theta_S = 0)$ (see figure 10(a)).

In the tunnelling limit, the spectrum of the superconductor with the gap function $\Delta_{k,1}$ contains a peak at the gap maximum and a feature at $|\Delta_s - \Delta_g|$ (see figure 9(b)). The spectrum of the superconductor with the gap function $\Delta_{k,2}$ contains a feature at the gap maximum, and a sharp peak at $\Delta_{k,2}(\theta_S = 0)$ (see figure 10(b)). The occurrence of the sharp peak at different positions in the conductance spectrum makes it possible to distinguish the tunnelling spectrum of the line-node gap from the point-node gap form using c-axis tunnelling data.

4. Conclusions

We have studied the c-axis and ab-plane tunnelling spectroscopy of s + g-wave superconductors. The observation of the predicted features in tunnelling measurements made for various junction orientations would, in principle, provide a way to study the detailed

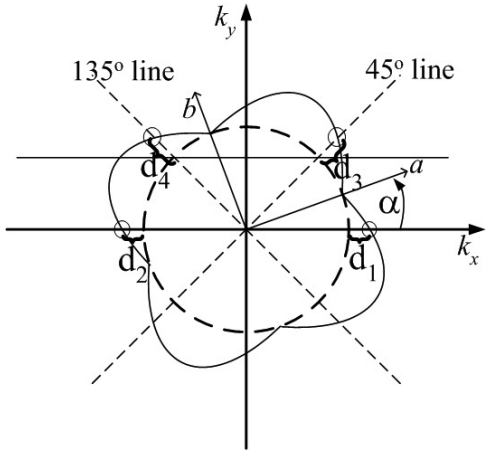

Figure 8. This picture shows a sketch of the gap function in the momentum space, when $\alpha \neq 0, \pi/4$. The dashed circle is the contour of the Fermi surface projected on the $k_x k_y$ plane. The solid curve represents the gap function. The two dashed lines are the $\phi_S = \pi/4$ and $3\pi/4$ lines. The solid horizontal line above $k_y = 0$ is the line of constant k_y at $\phi_S = \pi/4$ on the Fermi surface. This line cuts the Fermi surface at two points on the plane. Note that $d_1 = d_2$ (the magnitudes of the gap of the two excitations when $\phi_S = 0$) and $d_3 = d_4$ (the magnitudes of the gap the two excitations when $\phi_S = \pi/4$).

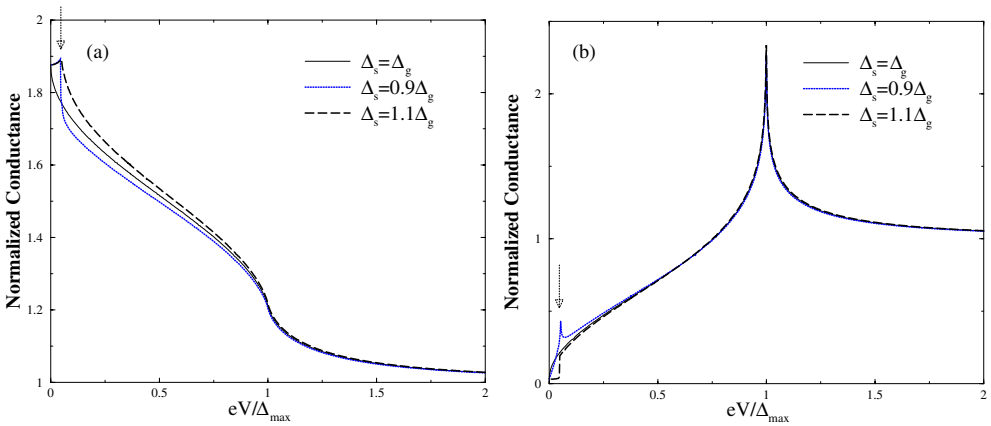

Figure 9. *c-axis tunnelling junctions.* The plots of the normalized conductance spectra for (a) $Z = 0$ and (b) $Z = 3$ in case of the gap $\Delta_{k,1} = \Delta_s - \Delta_g \cos 4(\phi_S \mp \alpha)$. The arrows indicate a feature occurring at $|\Delta_s - \Delta_g|$.

momentum dependence of an s + g-wave superconducting gap. In borocarbides, the presence of an s + g-wave gap function having either line or point nodes has been suggested. Directional tunnelling spectroscopy would help to determine whether either form of the superconducting gap is correct.

We can distinguish the *c*-axis tunnelling spectra of a superconductor with line nodes from the spectra of a superconductor with point nodes. In the tunnelling limit, the *c*-axis tunnelling conductance spectrum of a line-node superconductor contains a sharp peak at the gap maximum, whereas in the spectrum of a point-node superconductor a sharp peak occurs at the value of the gap function along the *c* axis.

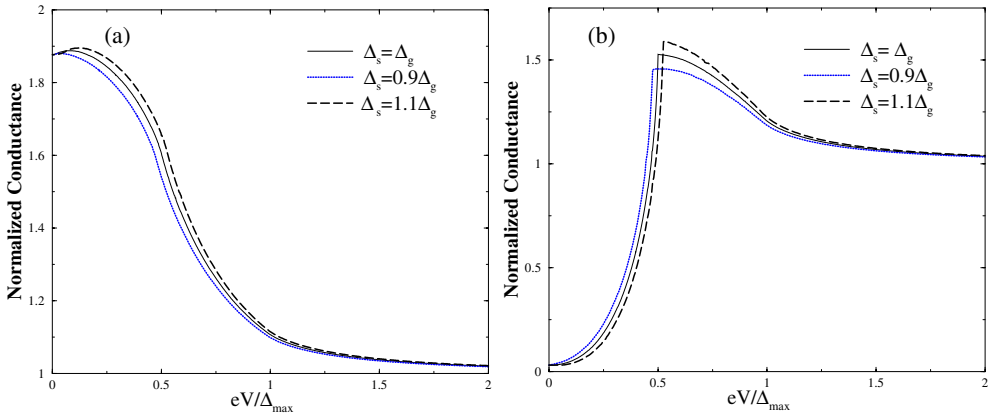

Figure 10. *c-axis tunnelling junctions.* The plots of the normalized conductance spectra for (a) $Z = 0$ and (b) $Z = 3$ in case of the gap $\Delta_{k,2} = \Delta_s - \Delta_g \sin^2\theta_S \cos 4(\phi_S \mp \alpha)$.

The ab-plane tunnelling spectra may be used to map out the magnitude of the gap function in the plane. The conductance spectrum of the ab-plane tunnelling junction is strongly dependent on the junction orientation. Two features in the spectrum appear at energies equal to the magnitude of the superconducting gap in two momentum directions: one is the direction parallel to the interface normal and the other is the direction making a $\pi/4$ angle with the interface normal. It is worth noting that these features are more prominent in the spectrum of the superconductor with line nodes than in the spectrum of the superconductor with point nodes, although this subtle distinction may not be observable especially at finite temperatures.

Acknowledgments

We would like to thank M B Walker for valuable discussions and comments. Also, PP would like to thank the Thailand Research Fund (TRF, grant No TRG4580057) for financial support.

References

[1] Boaknin E *et al* 2001 *Phys. Rev. Lett.* **87** 237001
[2] Izawa K *et al* 2002 *Phys. Rev. Lett.* **89** 137006
[3] Izawa K *et al* 2001 *Phys. Rev. Lett.* **86** 1327
[4] Jacobs T *et al* 1995 *Phys. Rev.* B **52** 007022
[5] Yang In-Sang *et al* 2000 *Phys. Rev.* B **62** 1291
[6] Nohara M *et al* 1999 *J. Phys. Soc. Japan* **68** 1078
[7] Nohara M *et al* 2000 *Physica* C **341–348** 2177
[8] Nohara M *et al* 1997 *J. Phys. Soc. Japan* **66** 1888
[9] Pairor P and Walker M B 2002 *Phys. Rev.* B **65** 064507
[10] Maki K *et al* 2002 *Phys. Rev.* B **65** 140502
[11] Lee H C and Choi Han-Yong 2002 *Phys. Rev.* B **65** 174530
[12] Blonder G E *et al* 1982 *Phys. Rev.* B **25** 004515
[13] Hu C-R 1994 *Phys. Rev. Lett.* **72** 001526
[14] Kashiwaya S *et al* 1996 *Phys. Rev.* B **53** 002667